JOURNAL OF Materials CHEMISTRY

Synthesis of mixed manganites with high surface area by thermal decomposition of oxalates

Christophe Drouet and Pierre Alphonse*

CIRIMAT, UMR-CNRS 5085, Université Paul Sabatier, 118 route de Narbonne, 31062 Toulouse Cedex 04, France. E-mail: alphonse@chimie.ups-tlse.fr

Received 18th April 2002, Accepted 22nd May 2002
First published as an Advance Article on the web 5th September 2002

Mixed manganites exhibiting very large specific surface areas were synthesized by thermal decomposition of mixed oxalates in an oxygen-containing atmosphere. A close control of the reaction kinetics was found to be necessary in order to prepare reproducible materials due to the high exothermic character of the oxalate decomposition, otherwise local increases of temperature led to a fast uncontainable growth of the crystallites. The effects of the powder bed thickness, thermal conditions and partial pressure of oxygen were also investigated and it was shown that the fixed-bed processing method was not suitable for the reproducible synthesis of large amounts of material.

Introduction

The thermal decomposition of metal oxalates has been widely investigated in the last forty years[1–17] due to its ability to produce, depending on the atmosphere, either metallic or metal oxide particles. In particular, mixed oxalates have been extensively used for the preparation of mixed oxides at low temperature.[18] Among such oxides, nonstoichiometric manganites synthesized at 673–773 K have recently raised special interest in the materials science community.[19–21] Indeed, such oxides are cation-deficient and highly divided materials, and present specific surface areas higher than 100 $m^2\ g^{-1}$, which is a critical technological asset for the synthesis of high-density ceramics at reduced sintering temperatures.[22,23] In addition, nonstoichiometric nickel and nickel–copper manganites were lately revealed as very efficient catalysts for reactions such as CO total oxidation[24] and NO reduction.[25]

As was pointed out before by Dollimore,[5] the decomposition process for transition metal oxalates strongly depends on the reducibility of the metallic cation involved. With cations presenting a low reducibility, like Zn^{2+} or Mn^{2+}, the decomposition leads to the corresponding metal oxide following the reaction scheme:

$$MC_2O_4 \rightarrow MO + CO + CO_2 \quad (1)$$

while with more reducible cations like Ni^{2+} or Cu^{2+} the decomposition produces the metal:

$$MC_2O_4 \rightarrow M + 2CO_2 \quad (2)$$

Both reactions are endothermic. But in the first case (reaction (1)), in the presence of oxygen, the oxidation of CO to CO_2 could occur:

$$CO + \tfrac{1}{2}O_2 \rightarrow CO_2 \quad (3)$$

If the metal oxide MO acts as a catalyst, this reaction could actually happen even under very low partial pressure of oxygen.

In the second case (reaction (2)), in the presence of oxygen, the metal M is oxidized:

$$M + \tfrac{1}{2}O_2 \rightarrow MO \quad (4)$$

Finally, since these oxidations are very exothermic, the overall decomposition reaction is exothermic too.

This work is aimed at determining whether, how and to what extent such an exothermic character of the overall decomposition reaction of mixed oxalates can affect the reproducible preparation of mixed oxides with high surface areas. Special interest has been devoted to manganese-, nickel- and copper-containing oxalates and oxides due to their recent implication in the catalytic processes mentioned above. The effect of a control of the kinetics of the decomposition reaction is investigated. In particular, we report how experimental parameters such as atmosphere composition, temperature and sample mass, can determine, mainly through alteration of the reaction kinetics, the microstructural characteristics of the final oxides. In this study, the thermal behavior of the overall process is discussed in a qualitative way only, because, to our knowledge, no reliable thermodynamic data are available to-date on the decomposition of such mixed oxalates.

Experimental

Preparation of mixed oxalates

Mixed oxalates $Ni_{x/3}Cu_{y/3}Mn_{(3-x-y)/3}C_2O_4{\cdot}nH_2O$ were precipitated at room temperature by quick introduction of an aqueous solution of nickel, copper and manganese nitrates (Prolabo RP Normapur™ analytical reagents; nitrate concentration: 0.2 M) into an aqueous solution of ammonium oxalate (Prolabo RP Normapur™) 0.2 M under vigorous stirring. After 30 minutes, the precipitate was allowed to settle, filtered, thoroughly washed with deionized water and dried in air at 90 °C.

Thermal decomposition of oxalates

The thermal decomposition of such oxalates was carried out in vertical tubular fixed-bed flow reactors under atmospheric pressure. According to the amount of sample, the internal diameter was in the 1–4 cm range. The flow rate of the inlet gas was generally set at 80 $cm^3\ min^{-1}$; the contact time was in the 0.1–2 s range. The gas flowing out of the reactor was simultaneously analyzed by mass spectrometry using a LEYBOLD INFICON Transpector H200M apparatus. The temperature of

 DOI: 10.1039/b203777g

the reacting solid was recorded by a probe directly in contact with the powdered sample.

Characterization of oxalates and oxides

The crystallographic structures of the oxalates and oxides were investigated by X-ray diffraction with a SIEMENS D501 diffractometer using copper Kα wavelength ($\lambda_{Cu} = 0.15418$ nm).

The chemical compositions were determined by atomic absorption and ion chromatography (DIONEX DX100, cationic column type CS-5).

The nitrogen adsorption/desorption isotherms were recorded at 77 K with a MICROMERITICS Accusorb 2100 apparatus. The specific surface areas of the samples were determined from the adsorption isotherms using the Brunauer–Emmett–Teller (BET) method. Transmission electron microscopy (TEM) analyses were performed using a JEOL 2010 (200 kV) microscope and scanning electron microscopy (SEM) analyses were done on a JEOL JSM 6400.

Thermal analyses

Thermogravimetric (TG) and differential thermal (DT) analyses were carried out on a SETARAM TG-DTA 92 thermobalance using 20 mg of sample. Alpha alumina was chosen as a reference.

The level of nonstoichiometry (noted δ) of the oxides $Ni_xCu_yMn_{3-x-y}O_{4+\delta}$ resulting from the thermal decomposition of mixed oxalates was evaluated from temperature-programmed-reductions monitored by thermogravimetric and gas chromatographic analyses. These experiments were carried out in a vertical plug-flow reactor. The mass variation of the oxide (initially 60 mg) was followed with a CAHN D200 thermobalance. The sample was first outgassed (1 Pa) at room temperature for 1 hour and the reactor was then filled with argon, maintaining a flow of 15 $cm^3\ min^{-1}$. The temperature was then increased linearly with a heating rate of 5 K min^{-1} up to 900 K. Every 120 s, the gas flowing out of the reactor was sampled and analyzed by gas chromatography (SHIMADZU GC-8A, molecular sieve 13X). The integration of the chromatographic data relative to the oxygen released upon heating the oxides in argon enabled us to evaluate δ. The accuracy of this technique was checked by heating in argon a known quantity of the stoichiometric oxides Mn_2O_3 (synthesized by thermal decomposition of manganese oxalate in air at 700 °C) and CuO (99%, Prolabo RP Normapur™) and determining the amount of oxygen released during their reduction to Mn_3O_4 and Cu_2O respectively. The final products were identified from their X-ray diffraction pattern. The experimental values obtained for the mass loss as well as for the amount of released oxygen were close to 99% of the theoretical value, which undoubtedly validates this technique. Such experiments are reproducible with a relative error of *ca.* 2% and have the advantage of allowing the nonstoichiometric oxygen to be selectively quantified, unlike other techniques based solely on the overall mass variation.

Results and discussion

Structure and characterization of the oxalates

As far as the crystallographic structure is concerned, both manganese oxalate and nickel oxalate belong to the so-called "magnesium series". This family of compounds consists of dihydrated oxalates $MC_2O_4{\cdot}2H_2O$ where the cation M^{2+} stands for Mg^{2+}, Mn^{2+}, Fe^{2+}, Co^{2+}, Ni^{2+}, or Zn^{2+}.[26,27] Two extreme atomic dispositions have been uncovered for these oxalates, namely the α and β forms, differing from each other in the arrangement of oxalate chains $(MC_2O_4)_n$ in the structure. Under the experimental conditions used here, manganese oxalate crystallizes in the α form. This

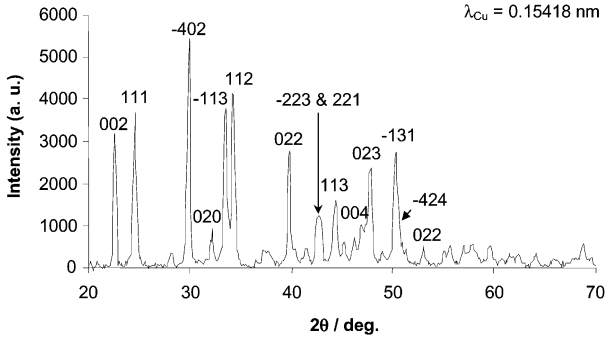

Fig. 1 XRD pattern for the mixed oxalate $Ni_{0.24}Cu_{0.12}Mn_{0.64}C_2O_4{\cdot}2H_2O$ indexed in α form (monoclinic *C*2/*c*: 15).

humboldtine-type allotropic variety can be described by the space group *C*2/*c*. The crystallographic system involved here is monoclinic, however the unit cell can also be viewed as pseudo-orthorhombic.[28,29] Nickel oxalate crystallizes in the β form (space group *Cccm*, orthorhombic system).[30] Copper oxalate has a different crystalline structure. Fichtner-Schmittler[31,32] determined the monoclinic structure of copper oxalate (space group $P2_1/c$) in the case of *ordered* crystals, but the most common *disordered* crystals of copper oxalate (containing stacking faults) may be described by an orthorhombic cell.

In a previous paper,[33] we reported that all attempts to synthesize a mixed copper–manganese oxalate by coprecipitation of copper and manganese nitrates with ammonium oxalate had failed. However, in that same study we showed that addition of nickel nitrate in the initial solution enabled the preparation of mixed oxalates $Ni_{x/3}Cu_{y/3}Mn_{(3-x-y)/3}C_2O_4{\cdot}nH_2O$ provided that $x_{Ni} \geqslant 0.1$. These findings indicated that the synthesis of mixed oxalates containing both copper and manganese was possible if nickel was also present in the structure. The allotropic variety, α or β, of such ternary Ni–Cu–Mn oxalates was then found to depend closely on their chemical composition, and particularly on their manganese content. X-Ray diffraction patterns for ternary oxalates with high manganese contents could be indexed in the α form whereas the β form was observed for low manganese contents. The pattern obtained for the oxalate $Ni_{0.24}Cu_{0.12}Mn_{0.64}C_2O_4{\cdot}2H_2O$ is reported in Fig. 1 as an example; it can easily be indexed in the α form. However, it should be noted that a progressive evolution of the structure of these ternary oxalates from α to β was evidenced for decreasing manganese contents.

Analysis of the oxalates by scanning electron microscopy (SEM) showed that Ni–Mn oxalates were composed of pseudo-octahedral particles whose size distribution was rather narrow, with an average particle size of about 5 μm (Fig. 2A). On the other hand, the morphology of the Ni–Cu–Mn oxalates (Fig. 2B) was found to be less regular, with a broader particle size distribution, and the octahedral shape was highly altered. Hence, the introduction of copper was found to deteriorate the morphology of Ni–Mn oxalates. This point had already been suspected by Fritsch.[34]

The question was whether these particles were microcrystalline or composed of single crystals. The determination of the BET surface area of these oxalates could have given us valuable information about their microstructure. Unfortunately, it was impossible to outgas the surface of these oxalates because of their high tendency to lose their structural water under vacuum, from room temperature (Fig. 3), which would lead to a strong alteration of the morphology.

Another way to estimate the crystallite size of such oxalates was to measure the broadening of X-ray diffraction lines using Scherrer's technique.[35] For the X-ray diffraction pattern presented in Fig. 1, this method yielded a mean particle size of about 30 nm, going in favor of microcrystalline particles.

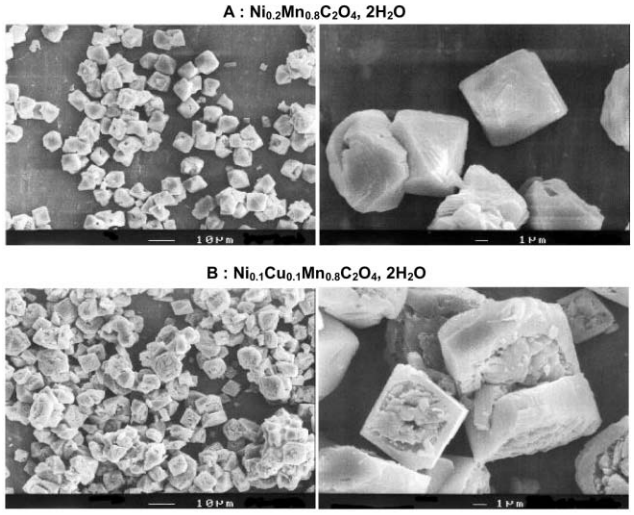

Fig. 2 SEM micrographs of mixed Ni–Mn (A) and Ni–Cu–Mn (B) oxalates.

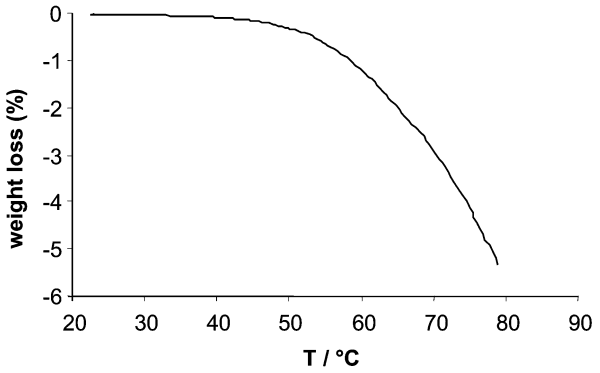

Fig. 3 TG of $Ni_{0.13}Cu_{0.21}Mn_{0.66}C_2O_4{\cdot}2H_2O$ under vacuum (4.5 Pa).

Thermal decomposition of mixed oxalates

When mixed manganites were prepared according to the "classical" way, which consisted of heating the oxalate powder (spread on a low-rimmed alumina pan) inside a conventional chamber furnace and under a dynamic air atmosphere, we noticed that the oxide characteristics strongly depended on the initial amount of oxalate used. In order to clarify this point, we introduced a temperature probe into the powder and analyzed the gaseous composition immediately above the sample by mass spectrometry. These measurements revealed that i) as the decomposition rate reached its maximum the temperature of the sample was several tens of a degree higher than that of the furnace and ii) the atmosphere above the reacting solid could contain a large proportion of carbon dioxide (more than 90% in some cases). In order to allow a better contact between the dynamic atmosphere and the oxalate powder, the thermal decomposition was then carried out in vertical tubular fixed-bed flow reactors. The temperature of the solid was accurately recorded by a probe placed in the powder. The outlet gas concentrations were determined by mass spectrometry. Most of the results reported below have been obtained with the ternary oxalate $Ni_{0.13}Cu_{0.21}Mn_{0.66}C_2O_4{\cdot}2H_2O$. The TG/DTA curves recorded for the decomposition of 0.02 g of this oxalate in an air atmosphere (heating rate of 150 °C h^{-1}) showed (Fig. 4) that the dehydration (first mass loss observed) and decomposition (second mass loss) processes were separated by about 100 °C. The decomposition of the anhydrous oxalate (second mass loss) started at 240 °C and ended at 300 °C. The specific surface area of the decomposition residue was larger than 100 m^2 g^{-1}.

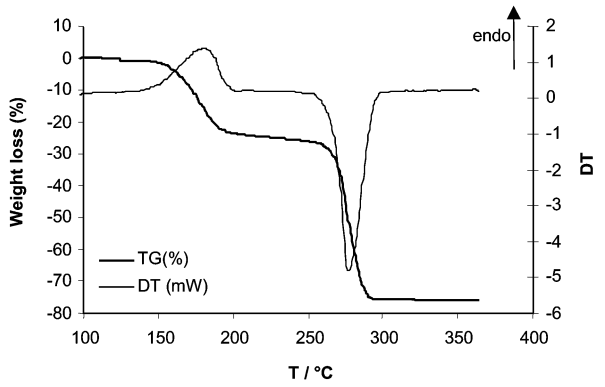

Fig. 4 TG and DTA profiles for thermal decomposition of $Ni_{0.13}Cu_{0.21}Mn_{0.66}C_2O_4{\cdot}2H_2O$ (heating rate 150 °C h^{-1}, m = 0.02 g).

When the decomposition of 0.12 g of this oxalate was carried out in a tubular reactor (air atmosphere, heating rate of 150 °C h^{-1}, contact time of 10^{-1} s) the reaction was completed in about 120 s. The recorded sample temperature as the decomposition rate reached its maximum was more than 100 °C higher than its expected value, the carbon dioxide partial pressure exceeded 45% and the oxygen concentration dropped below 2% (Fig. 5). Such findings show that, in that last case, the decomposition reaction went out of control, leading to a fast increase of the temperature (probably locally higher than that recorded) and, in turn, to an uncontrolled growth of the crystallites indicated by a specific surface area for the resulting oxide of only 25 m^2 g^{-1}. In order to slow the kinetics of the reaction, the effect of a decrease of the heating rate was investigated. However, a kinetically controllable decomposition was reached only when the reaction was carried out isothermally at a temperature close to 230 °C.

Under non-isothermal conditions, the decomposition of a small amount of oxalate (0.02 g) was completed in about 1200 s and ten times faster with 0.12 g of sample. It is worthwhile

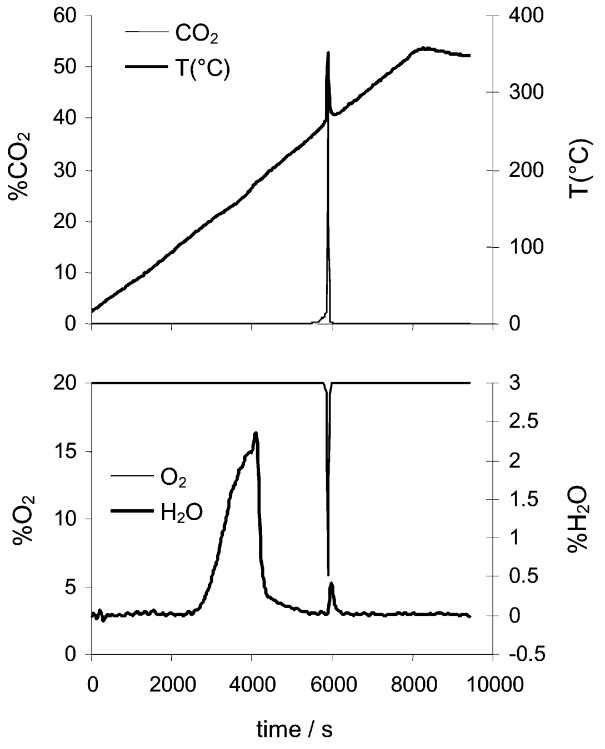

Fig. 5 Variation of recorded sample temperature and outlet gas composition during thermal decomposition in fixed bed reactor of $Ni_{0.13}Cu_{0.21}Mn_{0.66}C_2O_4{\cdot}2H_2O$ (heating rate 150 °C h^{-1}, m = 0.12 g).

Table 1 Effect of oxalate ($Ni_{0.13}Cu_{0.21}Mn_{0.66}C_2O_4{\cdot}2H_2O$) mass on the decomposition process. Temperature of furnace = 230 °C; partial pressure of O_2 = 20%

Oxalate mass/g	Temperature for maximum rate/°C	%CO_2 for maximum rate	Specific surface area/$m^2\ g^{-1}$
0.12	231	0.5	380
0.25	233	1.2	380
0.40	236	3.4	370
0.45	337	71	9
0.50	282	91	12

noting that, even under isothermal conditions, the rate of the reaction still depended on the initial amount of oxalate. We carried out an isothermal decomposition in an air atmosphere, with increasing amounts of oxalate, at 230 °C, keeping other conditions identical. The temperature recorded during the maximum reaction rate shows (Table 1) that the reaction went out of control from 0.45 g of oxalate. Surprisingly, for 0.5 g both the temperature shift and the specific surface area of the oxide indicated that the reaction rate was lower than for 0.45 g. This could however be explained by the increase of the partial pressure of CO_2 as the amount of oxalate increases (Table 1). Indeed the presence of CO_2 inhibits the oxalate decomposition. For example we found that, using 0.12 g of oxalate and a heating rate of 150 °C h^{-1}, the decomposition began 16 °C higher when 8% of CO_2 was added to the gas flow. In order to keep controlling the reaction kinetics with a mass of oxalate above 0.5 g (in the same reactor), the temperature would have to be decreased to 220 °C, which would lead to highly prolonged reaction times. In that case, a solution to this problem could be to use a reactor with a larger diameter and work with a higher flow rate. However, our observations showed that the thickness of the powder bed in the reactor was also a crucial parameter for the reaction kinetics to be controllable. It was found that such a control of the kinetics was only possible to achieve when the diameter of the reactor was chosen (according to the oxalate mass) so that the thickness of the solid bed was less than 2 mm. In such conditions, we synthesized mixed oxides presenting specific surface areas close to 400 $m^2\ g^{-1}$ from 4 g of oxalate. Note that fixed-bed reactors are not suitable for preparing large, reproducible, amounts of powder. Probably in that case fluidized-beds reactors should be more appropriate.

Since the exothermic character of the overall decomposition is due to oxidation reactions, another way of controlling its kinetics would be to modify the partial pressure of oxygen. Indeed, for the same initial mass of oxalate (here 0.5 g), the variation with time of the CO_2 concentration was shown to be highly dependent on the partial pressure of oxygen (Fig. 6), the initial reaction rate being directly linked to the O_2 concentration.

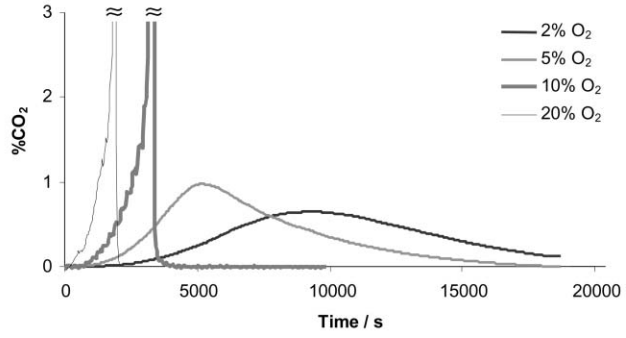

Fig. 6 Influence of partial pressure of O_2 on the thermal decomposition in fixed-bed reactor of $Ni_{0.13}Cu_{0.21}Mn_{0.66}C_2O_4{\cdot}2H_2O$ (T = 230 °C, m = 0.50 g).

Table 2 Kinetic expression for nucleation and growth models

Reaction mechanism	Kinetic expression
Avrami–Erofeev nuclei growth [36, 37]	$-\ln(1-\alpha) = kt^n$
Prout–Tompkins [38]	$\ln\frac{\alpha}{1-\alpha} = kt$
Mampel contracting-sphere [39]	$1-(1-\alpha)^{1/3} = kt$

Kinetic analysis of the experimental data

Integration and normalization of the experimental curves %CO_2 = f(t) enabled us to draw a set of α = f(t) curves where α stands for the fractional extent of the reaction. The overall shape of these curves was sigmoid so that we analyzed the data according to two different models: Avrami–Erofeev[36,37] and Prout–Tompkins[38] (see Table 2). In all cases, the best fit over the widest range of α was reached with the Avrami–Erofeev equation, and the corresponding parameters are given in Table 3 for some samples. For experiments run at 230 °C, the partial pressure of oxygen seemed to have a limited influence on the value of n. Indeed, at 230 °C, the slope (n) of the curve $\ln(-\ln(1-\alpha)) = f(\ln(t))$ was found close to 3 for all three samples No. 1, 2 and 3 corresponding to varying oxygen partial pressures. Note that the fit obtained for sample No. 1 was remarkable since, in the range α = 0 to 1.00, a correlation coefficient of 0.998 was attained (Fig. 7). The Avrami–Erofeev model with n = 3 could correspond to first-order formation, throughout the particles, of nuclei undergoing three-dimensional growth at constant rate, and coalescing when they overlap.

For experiments run at 220 °C, the parameters of the Avrami–Erofeev model were noticeably modified, *i.e.* the value of α_m (corresponding to the maximum rate) was *ca.* 0.3 rather than close to 0.4 and the slopes of the corresponding curves were decreased to *ca.* 2. Generally speaking, the fit obtained with the Avrami–Erofeev model for low reaction rates was less satisfying. In those cases, for α values above 0.12 a very good fit (correlation coefficient: 0.999 in case of samples No. 4 and 6) was found when applying the Mampel[39] contracting-sphere model (see Table 2). Hence, at low temperature, it seems that during the initial acceleratory period the nucleation and growth are more or less limited to the surface of crystallites. For α values close to 0.1, all the nuclei overlap and the reaction follows the Mampel contracting-sphere model.

However, deviations from the model could also be explained by the formation of carbonate species resulting from the interaction of carbon dioxide (produced during the decomposition) with large-surface-area oxide particles already formed. This will be discussed in the next paragraph.

Structure and characterization of the oxides

X-Ray diffraction analysis of the products resulting from isothermal decompositions of oxalates at 220 or 230 °C indicated that these were almost amorphous compounds. However, the principal lines of the cubic spinel structure (space group *Fd*3*m*) were clearly identifiable (Fig. 8, pattern A). It was thus possible to calculate the corresponding cell parameter (a),

Table 3 Summary of parameters for Avrami–Erofeev fitting *i.e.* plot of $\ln[-\ln(1-\alpha)]$ *vs* $\ln(t)$, α_m is the point of maximum rate, the slope is the value of n in Avrami–Erofeev equation given in Table 2

Sample	Oxalate mass/g	O_2 partial pressure (%)	T/°C	α_m	Slope	Correlation coefficient	α range
1	0.25	20	230	0.38	3.01	0.998	0.00–1.00
2	0.50	5	230	0.36	3.09	0.987	0.03–0.95
3	0.50	2	230	0.39	3.00	0.997	0.00–0.90
4	0.50	20	220	0.33	2.27	0.991	0.02–0.98
5	0.50	20	220	0.32	2.05	0.993	0.03–0.95
6	0.50	40	220	0.31	2.11	0.992	0.02–0.98

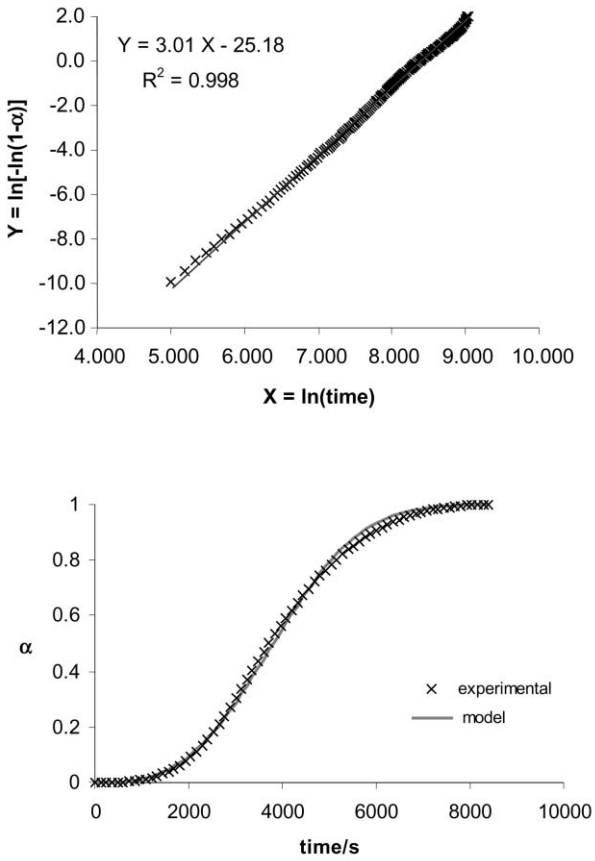

Fig. 7 Kinetic analysis of the thermal decomposition of $Ni_{0.13}Cu_{0.21}Mn_{0.66}C_2O_4{\cdot}2H_2O$ using the Avrami–Erofeev equation (O_2 20%, $T = 230$ °C, $m = 0.25$ g): (A) plot of $\ln[-\ln(1-\alpha)]$ *vs.* $\ln(t)$ for α range from 0 to 1.0; (B) comparison of experimental data with model curve for the best fitting parameters ($n = 3.01$ and $k = 1.16 \times 10^{-11}$).

and the value $a = 0.832 \pm 0.005$ nm was found from pattern A. As was done above for the oxalates, the crystallite size of these oxides could be evaluated from Scherrer line broadening measurements. From the diffraction pattern A, we found a mean particle size of about 4 nm.

Upon heating such oxides in an inert atmosphere (argon), the spinel structure was retained and the growth of the crystallites was accompanied by the release of oxygen, leading at 700 °C to the corresponding stoichiometric oxide (pattern B in Fig. 8) for which the cell parameter was $a = 0.8395 \pm 0.0005$ nm.

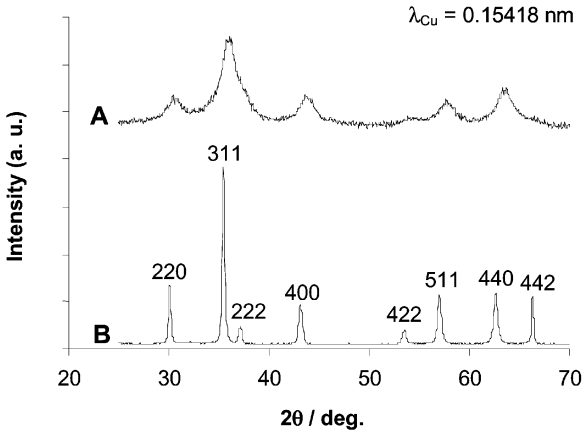

Fig. 8 XRD pattern for (A) nonstoichiometric oxide $Ni_{0.77}Cu_{0.35}Mn_{1.88}O_{4.43}$ prepared at low temperature and (B) stoichiometric oxide $Ni_{0.77}Cu_{0.35}Mn_{1.88}O_4$ resulting from heating A at 700 °C. B is indexed as a cubic spinel *Fd3m*(227).

Table 4 Effect of some synthesis parameters on the characteristics of oxides prepared from decomposition of $Ni_{0.13}Cu_{0.21}Mn_{0.66}C_2O_4{\cdot}2H_2O$ oxalate – gas flow rate = 80 cm^3 min^{-1}

Sample	Sample mass/g	O_2 partial pressure (%)	Temp. of plateau/ °C	Specific surface area/m^2 g^{-1}	δ	Carbonates mass (%)
1	0.25	20	230	380	0.5	2.8
2	0.5	2	230	370	0.5	2.6
3	0.5	5	230	370	0.5	3.0
4	0.5	20	220	390	0.5	3.5
5	0.5	20	220	380	0.6	2.4
6	0.5	20	230	10	0.06	0.2
7	1.0	2	230	13	0.09	0.1
8	1.0	5	230	165	0.3	1.1
9	2.0	4	220	335	0.55	4.5
10	2.0	4	220	460	0.45	5.0

This point indicated that the oxides produced by thermal decomposition of oxalates at low temperature were initially nonstoichiometric. Such a nonstoichiometry can be explained by the presence of cations with larger oxidation states than in stoichiometric oxides,[19] implying the presence of cationic vacancies. The "degree" of nonstoichiometry of these oxides, δ, was determined by titration of the oxygen released during temperature programmed reduction experiments in argon. For example, the value $\delta = 0.43$ was found for the oxide corresponding to the diffraction pattern A (Fig. 8). Surprisingly, we observed that δ did not depend on the partial pressure of oxygen (in the range 2 to 20%) during the decomposition (see Table 4). On the other hand, a close relationship was evidenced between δ and the specific surface area of the oxides: only large surface-area oxides presented elevated degrees of nonstoichiometry.

From nitrogen adsorption/desorption isotherms, we calculated the related pore size distribution using the BJH method.[40] This distribution was found to be unimodal (Fig. 9), with a pore diameter close to the average particle size. Moreover, from the values of the cell parameter of the oxides, an evaluation of the theoretical density (referred as ρ) was possible and, assuming as a first approximation that all particles were spherical and had the same diameter (D), the related specific surface area S could be calculated using the equation:

$$S = \frac{6}{\rho D}$$

In all cases the calculated surface areas were close to the experimental values derived from BET isotherms. These findings show that the porosity of such oxides does not correspond to internal porosity of the crystallites but to some

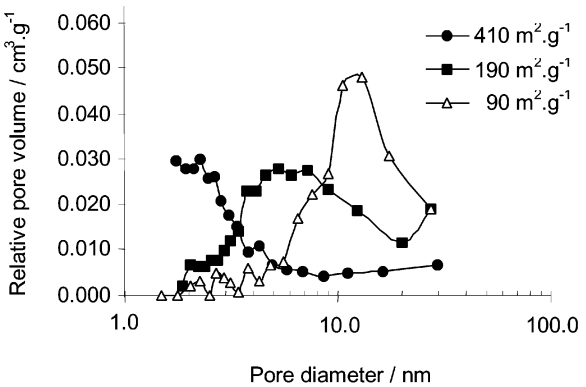

Fig. 9 Pore size distribution calculated by the BJH method[40] for nonstoichiometric oxides $Ni_{0.73}Cu_{0.82}Mn_{1.45}O_{4.6}$ (410 m^2 g^{-1}), $Ni_{0.73}Cu_{0.82}Mn_{1.45}O_{4.3}$ (190 m^2 g^{-1}), $Ni_{0.73}Cu_{0.82}Mn_{1.45}O_{4.25}$ (90 m^2 g^{-1}).

inter-particle porosity linked to the unoccupied space remaining between the crystallites.

The mass losses observed from TG analyses run on the oxides were higher than those expected considering only a release of oxygen. Mass spectrometry analyses revealed that, during these experiments, water vapor was formed between 200 and 300 °C as well as carbon dioxide between 350 and 500 °C. However, only a small mass loss (generally less than 0.2%) could be attributed to the formation of water, which most likely arose from the decomposition of residual surface hydroxides. Carbon dioxide was probably produced from the decomposition of carbonate species, the temperature range 300–440 °C indeed corresponds to the decomposition domain of manganese carbonate.[41] One could thus assume that, during the oxalate decomposition, part of the CO_2 produced could have reacted with some large-surface-area oxide particles already formed to give carbonate species, according to a reaction of the type:

$$MnO + CO_2 \rightarrow MnCO_3 \quad (5)$$

With this assumption, the percentage of such carbonates contained in the oxides was calculated and added in Table 4. As can be seen, this amount of carbonate was found to increase with the specific surface area, as well as (as a general trend) when the decomposition rate decreased. Indeed, samples No. 9 and 10 were found to contain more carbonate than the other samples tested. For these two samples, a higher initial mass of oxalate was used, with the same flow rate, leading to a higher partial pressure of CO_2 during the decomposition. These findings are in good agreement with the assumption that some carbonate species were formed according to reactions like reaction (5). Finally, it is noteworthy pointing out that oxides synthesized by isothermal decomposition at 220 or 230 °C did not seem to be affected by heating in an air atmosphere up to 350 °C: the specific surface areas, diffraction patterns and nonstoichiometry levels remaining the same. This could be linked to the fact that carbonate decomposition only begins above 350 °C.

Conclusion

The thermal decomposition of mixed oxalates in an oxygen-containing atmosphere was found to be an adequate synthesis route to prepare mixed manganites with very large surface areas. We demonstrate in this work that it is essential to maintain a close control of the reaction kinetics to ensure that the synthesis process gives reproducible materials. However, the strong exothermic character of the overall decomposition makes this control rather difficult to achieve and, as soon as the reaction gets out of control, temperature locally rises quickly, leading in turn to a rapid growth of the crystallites. In an air atmosphere, in fixed-bed reactors, the thickness of the bed must be less than about two millimeters to keep the reaction under control, even in isothermal conditions. By decreasing the temperature or the partial pressure of oxygen, it is possible to decrease the reaction rate but only to a certain extent. This work also points out that the fixed-bed processing method could not be used for the reproducible synthesis of large amounts of materials. In that case, fluidized-bed reactors would probably be more suitable.

References

1 D. Broadbent, D. Dollimore and J. Dollimore, *J. Chem. Soc.*, 1966, 279.
2 K. Nagase, K. Sato and N. Tanaka, *Bull. Chem. Soc. Jpn.*, 1975, **48**, 439.
3 M. G. Usha, S. M. Rao and T. R. Narayanan Kutty, *Thermochim. Acta*, 1981, **43**, 35.
4 J. Mu and D. D. Perlmutter, *Thermochim. Acta*, 1981, **49**, 207.
5 D. Dollimore, *Thermochim. Acta*, 1987, **117**, 331.
6 D. Broadbent, J. Dollimore, D. Dollimore and T. A. Evans, *J. Chem. Soc., Faraday Trans.*, 1991, **87**, 161.
7 A. Coetzee, D. J. Eve and M. E. Brown, *J. Therm. Anal.*, 1993, **39**, 947.
8 A. Coetzee, M. E. Brown, D. J. Eve and C. A. Strydom, *J. Therm. Anal.*, 1994, **41**, 357.
9 S. Bosea, K. K. Sahua and D. Bhatta, *Thermochim. Acta*, 1995, **268**, 175.
10 A. K. H. Nohmana, H. M. Ismaila and G. A. M. Husseina, *J. Anal. Appl. Pyrolysis*, 1995, **34**, 265.
11 S. N. Basahela, A. A. El-Bellihib, M. Gabalb and H. M. El-Diefallaah, *Thermochim. Acta*, 1995, **256**, 339.
12 A. M. Donia, *Polyhedron*, 1997, **16**, 3013.
13 N. Routraa, S. Pattnaika and D. Bhatta, *Radiat. Phys. Chem.*, 1997, **49**, 89.
14 R. Majumdar, P. Sarkar, U. Ray and M. Roy Mukhopadhyay, *Thermochim. Acta*, 1999, **335**, 43.
15 A. K Nikumbh, A. E. Athare and S. K. Pardeshi, *Thermochim. Acta*, 1999, **326**, 187.
16 B. V. L'vov, *Thermochim. Acta*, 2000, **364**, 99.
17 S. Dash, R. Krishnan, M. Kamruddin, A. K. Tyagi and Baldev Raj, *J. Nucl. Mater.*, 2001, **295**, 281.
18 J. Robin, *Bull. Soc. Chim. Fr.*, 1953, 1078.
19 X. X.Tang, A. Manthiram and J. B. Goodenough, *J. Less Common Met.*, 1989, **156**, 357.
20 J. Töpfer and J. Jung, *Thermochim. Acta*, 1992, **202**, 281.
21 C. Laberty, P. Alphonse, J. J. Demai, C. Sarda and A. Rousset, *Mater. Res. Bull.*, 1996, **32**, 249.
22 W. H. Rhodes, *J. Am. Ceram. Soc.*, 1981, **64-1**, 19.
23 S. Inada, T. Kimura and T. Yamagushi, *Ceram. Int.*, 1990, **16**, 369.
24 C. Laberty, C. Marquez-Alvarez, C. Drouet, P. Alphonse and C. Mirodatos, *J. Catal.*, 2001, **198**, 266.
25 C. Drouet, P. Alphonse and A. Rousset, *Appl. Catal. B Environ.*, 2001, **33**, 35.
26 S. Caric, *Bull. Soc. Fr. Mineral. Cristallogr.*, 1959, **82**, 50.
27 J. P. Lagier, PhD Thesis, Paris, 1970.
28 H. Pezerat, J. Dubernat and J. P. Lagier, *C. R. Acad. Sci., Ser. C Paris*, 1968, **266**, 1357.
29 F. Mazzi and C. Garavelli, *Period. Mineral.*, 1957, **26**, 269.
30 R. Deyrieux, C. Berro and A. Péneloux, *Bull. Soc. Chim. Fr.*, 1973, **1**, 25.
31 H. Fichtner-Schmittler, *Cryst. Res. Technol.*, 1984, **19-9**, 1225.
32 H. Fichtner-Schmittler, *Monatsber. Dtsch. Akad. Wiss. Berlin*, 1968, **10**, 581.
33 C. Drouet, P. Alphonse and A. Rousset, *Solid State Ionics*, 1999, **123**, 25.
34 S. Fritsch, PhD Thesis, Toulouse, 1995.
35 A. L. Patterson, *Phys. Rev.*, 1939, **56**, 978.
36 M. Avrami, *J. Chem. Phys.*, 1939, **7**, 1103; M. Avrami, *J. Chem. Phys.*, 1940, **8**, 212; M. Avrami, *J. Chem. Phys.*, 1941, **9**, 177.
37 B. V. Erofeev, *C. R. Acad. Sci. URSS*, 1946, **52**, 511.
38 E. G. Prout and F. C. Tompkins, *Trans. Faraday Soc.*, 1944, **40**, 488.
39 K. L. Mampel, *Z. Phys. Chem., Abt. A*, 1940, **187**, 235.
40 E. P. Barrett, L. G. Joyner and P. P. Halenda, *J. Am. Chem. Soc.*, 1951, **73**, 373.
41 W. M. Shaheen and M. M. Selim, *J. Therm. Anal. Calorim.*, 2000, **59**, 961.